International Journal of Hyperthermia

ISSN: 0265-6736 (Print) 1464-5157 (Online) Journal homepage: http://www.tandfonline.com/loi/ihyt20

Laser ablation of the biliary tree: in vivo proof of concept as potential treatment of unresectable cholangiocarcinoma

Paola Saccomandi, Giuseppe Quero, Riccardo Gassino, Alfonso Lapergola, Ludovica Guerriero, Michele Diana, Alberto Vallan, Guido Perrone, Emiliano Schena, Guido Costamagna, Jaques Marescaux & Francesco M. Di Matteo

To cite this article: Paola Saccomandi, Giuseppe Quero, Riccardo Gassino, Alfonso Lapergola, Ludovica Guerriero, Michele Diana, Alberto Vallan, Guido Perrone, Emiliano Schena, Guido Costamagna, Jaques Marescaux & Francesco M. Di Matteo (2018): Laser ablation of the biliary tree: in vivo proof of concept as potential treatment of unresectable cholangiocarcinoma, International Journal of Hyperthermia, DOI: 10.1080/02656736.2018.1427287

To link to this article: https://doi.org/10.1080/02656736.2018.1427287

Accepted author version posted online: 11 Jan 2018.

Laser ablation of the biliary tree: *in vivo* proof of concept as potential treatment of unresectable cholangiocarcinoma

Paola Saccomandi[1, 2], Giuseppe Quero[1], Riccardo Gassino[3], , Alfonso Lapergola[4], Ludovica Guerriero[1], Michele Diana[1, 4], Alberto Vallan[3], Guido Perrone[3], Emiliano Schena[2], Guido Costamagna[1, 5], Jaques Marescaux[1, 4], Francesco M. Di Matteo[2]

1) IHU-Strasbourg, Institute of Image-Guided Surgery, Strasbourg, France

2) Campus Bio-Medico di Roma, Rome, Italy

3) Politecnico di Torino, Department of Electronics and Telecommunications, Turin, Italy

4) IRCAD, Research Institute against Digestive Cancer, Strasbourg, France

5) Università Cattolica del Sacro Cuore, Rome, Italy

Corresponding author: Paola Saccomandi

Email: paola.saccomandi@ihu-strasbourg.eu

Laser ablation of the biliary tree: *in vivo* proof of concept as potential treatment of unresectable cholangiocarcinoma

Abstract:

Objectives: The palliative treatment of cholangiocarcinoma is based on stent placement with well-known procedure-related complications. Consequently, alternative energy-based techniques were put forward with controversial long-term results. This study aims to evaluate the safety and effectiveness of biliary tree laser ablation (LA) in terms of: i) absence of perforation, ii) temperature increase, iii) induced thermal damage in *in vivo* models.

Materials and methods: The common bile duct and cystic ducts of two pigs were ablated with a diode laser (circumferential irradiation pattern) for 6 and 3 minutes at 7 W. Laser settings were chosen from previous *ex vivo* experiments. Local temperature was monitored through a fiber Bragg grating (FBG) sensor embedded into the laser delivery probe. Histopathological analysis of the ablated specimen was performed through *in situ* endomicroscopy, hematoxylin and eosin (H&E) and nicotinamide adenine dinucleotide (NADH) stains.

Results: Temperature reached a plateau of 53 °C with consequent thermal damage on the application area, regardless of laser settings and application sites. No perforation was detected macroscopically or microscopically. At the H&E stain, wall integrity was always preserved. The NADH stain allowed to evaluate damage extension. It turned out that the ablation spreading width depended on application time and duct diameter. *In situ* endomicroscopy revealed a clear distinction between ablated and non-ablated areas.

Conclusions: The temperature distribution obtained through LA proved to induce a safe and effective intraductal coagulative necrosis of biliary ducts. These results represent the basis for further experiments on tumor-bearing models for the treatment of obstructive cholangiocarcinoma.

Key words: biliary tree, intraductal laser ablation, thermometry, *in vivo* study, cholangiocarcinoma

Introduction

Cholangiocarcinoma is an aggressive adenocarcinoma which arises from the epithelial cells of the biliary tract and accounts for up to 20% of primary liver cancers [1]. At the time of diagnosis, most patients present at an unresectable stage (III or IV) [2]. This relates to an extremely poor prognosis, with a median survival ranging from 3 to 6 months [3] and a 5-year overall survival for stage III and IV patients of 10 and 0% respectively [2].

Therapeutic palliative solutions for unresectable conditions are mainly based on biliary decompression techniques [4]. As a result, multiple techniques of biliary decompression have been put forward. Among mechanical solutions, endoscopic stent placement is currently considered the treatment of choice in the palliation of unresectable obstructive cholangiocarcinomas. Either plastic or self-expandable metal stents (SEMSs) can be used to obtain an adequate biliary drainage. Plastic stents are effective, easily removable and replaceable. However, complications, such as occlusion and cholangitis, frequently occur after their placement, requiring repeated endoscopic disobstructive procedures and replacements [5]. Conversely, tumor tissue ingrowth, epithelial hyperplasia, biofilm deposition, and stent migration represent some of the main SEMSs drawbacks [6].

In order to reduce stent-related complications, different energy-based techniques have been put forward as alternative strategies. Radiofrequency ablation (RFA) alone or in combination with SEMSs positioning proved to be feasible. And yet, its long-term efficacy is still unclear. A comparison between RFA combined with SEMSs and SEMSs alone has been reported, with a statistically significant improvement in patency in the RFA group as demonstrated in other studies [7, 8]. However, post-procedural complications, such as biliary bleeding, pancreatitis, hemobilia, and cholangitis cannot be neglected [7].

Photodynamic therapy (PDT) was initially used in the treatment of biliary duct tumors with promising results in maintaining biliary patency [9, 10]. However, phototoxicity (which can last up to 6 weeks) [11] and cutaneous complications [12] are the most frequent clinical drawbacks. In addition, a recent multicenter

randomized study (Photostent-02) demonstrated a 61% excess of mortality risk in patients receiving PDT plus stenting as compared to stenting alone together with a reduced overall survival [13].

Over the last decades, the laser ablation (LA) technique has shown effectiveness in the clinical field. Promising results have already been demonstrated in minimally invasive palliative or potentially curative LA of hepatocellular carcinomas, liver metastases, and thyroid nodules [14, 15, 16, 17, 18, 19]. More recently, its application has been extended to the treatment of solid pancreatic tumors with promising preliminary results [20]. It can allow for the destruction of tumor cells by directing light energy into the tissue through optical fibers [18, 21]. The light energy is absorbed and converted into heat, and the subsequent increase in tissue temperature induces coagulative necrosis in the target [19, 22, 23]. The two main advantages of fiber-delivered laser light for this application are the following: i) the use of non-traumatic flexible thin needles, which make it possible to perform minimally invasive endoscopic procedures, ii) the possibility to customize the irradiation pattern to modulate temperature distribution in relation to tumor shape by properly micro-patterning the delivery fiber surface.

When thermal procedures are used for local treatment, the key factor to assess the effectiveness of therapeutic outcome is the induced thermal damage, which is related to the rise in tissue temperature. As a consequence, a system for real-time temperature monitoring is essential to optimize treatment effects. When using fiber-optic technologies, the sensing and the ablation system can be easily combined in order to measure local tissue temperature change during LA. Fiber Bragg grating (FBG) sensors are the most common tools for fiber-based thermometry in medical applications [24, 25]. Among the other well-known thermometric systems necessitating contact with the field, such as thermocouples, FBG sensors embed valuable features for the application specific to this scenario. For instance, thermocouples can present some concerns in their use during LA. As a matter of fact, their metallic conductors highly absorb the laser-emitted radiation, and this phenomenon induces an increase in local temperature, causing a significant overestimation of actual tissue temperature, which can raise up to 20°C [24, 26]. Additionally, FBG

temperature sensors can be inscribed directly into the delivery fiber core or bundled with it, in both cases leading to small-sized systems which can be easily guided towards the target via catheters and needles [27]. This feature makes the delivery-measurement system immune from electromagnetic interferences, and is compatible with magnetic resonance imaging (MRI) applications. Regarding the dynamic characteristics of FBG sensors, the response time of a grating (<0.3 mm diameter) embedded within a 1mm diameter needle is approximately 0.1 s (0.1 s to 0.3 s) [28, 29]. This value matches with the time constant of thermocouples with a diameter of 0.1 mm to 0.3 mm. As a result, FBG sensors provide a reasonably fast measurement, according to the specific medical application. Regarding the repeatability, modern optical spectrum interrogator systems offer wavelength repeatability of 1 pm, corresponding to 0.1 °C. Lastly, FBG sensors offer the advantage of providing a multi-point measuring system inside the same fiber. Several FBG sensors can be embedded within the core of the same fiber, reducing the invasiveness of the measure to a single insertion. The use of FBG sensors as temperature monitoring devices for thermal procedures has already been demonstrated in liver and pancreatic ablations, among others [30].

In spite of all the advantages reported and the clinical efficacy already demonstrated in the laser treatment of solid tumors, only *ex vivo* studies described biliary tree LA with promising results [31]. In this study, to the best of our knowledge, we report the first *in vivo* experiments of LA with temperature monitoring by means of an FBG sensor. This study aims to demonstrate the feasibility of biliary tree and cystic duct LA with a real-time temperature measurement. It would be the first step in the future perspective of introducing this technique into a clinical setting for the treatment of biliary obstructive malignant diseases.

Materials and methods

Light delivery and FBG sensing tool

The first step of the study consisted in the development of a suitable laser probe with an embedded FBG sensor to properly deliver a high-power laser beam to the tissue and simultaneously measure the induced temperature increase (Figure 1). The laser system was manufactured *ad hoc* in cooperation with a company (OPI Photonics, Turin, Italy). It is based on a high-power laser diode source at 940 nm combined with a probe built on a 44 0µm-core diameter multi-mode silica optical fiber. The irradiation pattern from the delivery fiber was optimized by properly patterning its lateral surface, for a length of about 1cm, through an exposure to a UV-laser light. In this manner, light can escape from the lateral surface in a controlled way (and not only from the tip as it happens in unmodified fibers), producing an almost cylindrical irradiation pattern [27]. An FBG (from Technica, inscribed in the core of a standard telecom grade 125 µm-diameter fiber with polyimide coating, central wavelength of 1557.5 nm) was placed in contact with the delivery fiber in correspondence to the irradiated region in order to monitor the induced tissue temperature. The two fibers were kept together by means of a 1.2 mm (external diameter) silica glass sealed capillary. The choice of the silica glass material (the same material as optical fibers) for this protective capillary is motivated by its low infrared light absorption. The entire system is controlled by a custom-made LabVIEW (National Instruments) software, which allows to monitor the laser status and to control parameters such as laser power and treatment time [27].

Tissue temperature variation measurement is obtained by analyzing the optical FBG response. When fed by a polychromatic light source, the grating acts as an optical filter; the reflected narrow spectrum is centered on a value known as the Bragg wavelength (λ_B) while all other wavelengths are transmitted. When FBG experiences a change in temperature, λ_B shifts linearly by about 10 pm/°C [25, 32]. An optical spectrum interrogator system (Micron Optics Hyperion Platform, Sensing Instrument si155, sampling rate: 10 Hz) was used to interrogate and detect any change in wavelength. The measured temperature data were

provided in real time during the experiments with the support of a dedicated software (MOI Enlight).

Figure 1.

Animal tests: study design and histopathological analysis

The experimental study was divided into two main parts: the *ex vivo* and *in vivo* tests.

Ex vivo experiments

The preliminary *ex vivo* tests aimed to define the laser settings to be used in the *in vivo* experiment. The main objective was to observe the power and time of application to be used to perform duct ablation without perforation. To do so, a fresh pig liver was used and a total of 4 ablations were performed in different portions of the common bile duct, at a mean distance of 1.5 cm between two consecutive ablations, in order to prevent overlapping. After intraductal laser probe introduction, ablations were performed from the upper to the lower part of the common bile duct. The laser power was delivered with values of 3 W, 5 W, and 7 W, for 2 min, and 7 W for 3 min. After LA, the evaluation of thermal damage was carried out by means of a histological analysis.

In vivo experiments

A total of 2 pigs underwent biliary tree LA. In agreement with the ethical principle of reduction, animals were included at the end of a different experimental protocol at the Image-Guided Surgery Institute (IHU) of Strasbourg, which received full approval from the Institutional Ethical Committee. All animals used in the experimental laboratory were managed according to French laws for animal use and care and according to the directives of the European Community Council (2010/63/EU) with respect to the 3R principles (Replacement, Reduction, and Refinement). Animals were humanely sacrificed at the end of the procedure.

After anesthesia, using 10cc of Propofol and 5cc of Esmeron (2% isoflurane was injected during the ongoing procedure), the 2 pigs (45-50 kg) underwent a

laparotomy. After recognition of the hepatic hilum structures (common bile duct, hepatic artery, and portal vein), both the common bile duct and the cystic duct were carefully isolated. Firstly, a 1 cm transverse incision of the common bile duct in its middle lower portion was performed. The laser applicator embedding the FBG sensor was then carefully inserted inside the duct, and LA was performed (Figure 2).

Figure 2.

After common bile duct ablation, the same procedure was then performed after insertion of the laser applicator into the cystic duct through a 1cm incision. Protective glasses were worn by all operators during LA.

A total of 4 LA procedures (one on the common bile duct and one on the cystic duct of each pig) were performed. Our choice to also perform LA on the cystic duct aimed to understand the laser effects on ducts of minor caliber, mimicking intrahepatic bile ducts, and to easily place the laser applicator under plain visual guidance. Indeed, in humans, the diameter of the common bile duct varies from 6 mm to 8 mm [33] while the diameter of the cystic duct ranges from 1 mm to 5 mm [33].
Based on LA results obtained in the *ex vivo* model (described in the 'Results of the *Ex vivo* experiment' section), a power value of 7 W was applied for 3 min and 6 min, on both ducts. Simultaneously, the rise in LA-induced ductal temperature was monitored by means of the FBG sensor.

A first-sight evaluation after LA was crucial to evaluate external ablated areas and potential surrounding tissue damage. In addition, at the end of each LA, the common bile duct and the cystic duct were both resected as a unique specimen 'en bloc' with the gallbladder. After specimen removal, the ablated areas were carefully resected including thermal damage with at least 1cm of superior and inferior normal tissue margins. Histopathological analysis was performed to assess thermal damage.

On each treatment site, a histological *in situ* evaluation was also obtained before and after LA using a confocal endomicroscopy system (Cellvizio®, Mauna Kea Technology, Paris, France), in order to assess the LA effect. To

obtain confocal images, a 5mL sodium fluorescein solution (Fluocyne 10%, SERB Laboratories) was injected intravenously at the beginning of each surgical procedure, and images were obtained with the Gastroflex UHD probe, (240μm-diameter FoV, 1μm resolution, 55-65μm confocal depth [36]). Video recording of the endomicroscopy analysis was performed before and after the ablation for each laser application. First, the *in situ* visual confocal endomicroscopy evaluation before LA allowed to assess the normal structure of the bile and cystic ducts. The immediate post-LA analysis aimed to test the feasibility of confocal endomicroscopy in the recognition of ablation areas.

As already reported in other studies, an endomicroscopic grading system based on the amount of cell shedding on good quality images was used to objectively evaluate the thermal damage induced [37, 38]. Images from the recorded videos were analyzed through the image processing tool of Matlab® in order to distinguish between pre-ablation and post-ablation scenarios.

The definitive histological analysis of the ablated areas was performed using two staining techniques, i.e. hematoxylin and eosin (H&E), as well as nicotinamide adenine dinucleotide (NADH) diaphorase stains. Particularly, this last technique helps to evaluate the ablated areas through the assessment of metabolic damage, because the vital tissue where oxidative metabolism is preserved gets selectively colored in blue. This characteristic pigmentation is lost within the areas of coagulative necrosis where NADH activity was lost. The histological analysis to evaluate ablation damage was performed using a light microscope (Zeiss Axiophot).

The histopathological analysis resulted useful also to evaluate the internal diameter of the ducts undergoing LA. For each duct, the two main axes were measured by means of the AxioVision Rel 4.8 image analysis software used to acquire sliced pictures at a 5x enlargement.

Results

Ex vivo experiments

Thermal damage induced in the *ex vivo* organ was assessed via a histological analysis. At 3 W, 5 W, and 7 W for 2 min, no thermal damage was observed at macroscopic evaluation. When maintaining P at 7 W and varying the application time up to 3 min, an ablated area was detected at histology while no injury to surrounding tissues occurred. For this reason, 7 W for 3 min was used as a starting laser setting in the *in vivo* experiment. Figure 3 shows the histological pictures of normal common bile duct and cystic ducts, before (Figures 3A and 3B) and after (Figures 3C and 3D) the ablation treatment at 7 W for 3 minutes.

Figure 3.

In vivo experiments

Figure 4 reports temperature trends during the *in vivo* experiment at 7 W for 3 min (Figures 4A and 4B), as well as the test which lasts 6 min (Figures 4C and 4D) for common bile duct and cystic duct respectively.

Figure 4.

In all experiments, the temperature overcame the value of 53 °C after about 50 s from turning the laser on, and was maintained along the heating phase, up to the moment the laser was turned off. The probe was then removed from the ducts, and the measured temperature decreased below the initial systemic temperature. Fluctuations in the measured values could be related to three main factors: 1) the surgeon's physiological hand tremor, 2) the animals' breathing movements, and 3) the possible discontinuous bile flux in the ducts. In order to minimize the influence of these factors in the global evaluation of temperature trends, mean temperature values (Tmean) measured via the FBG after 50 s from turning the laser on was determined. For each of the 4 trends shown in Figure 4, Tmean was calculated as the mean value of the measured T from 50 s from turning the laser on until the end of LA.

After the H&E stain analysis, the diameters of the ducts were measured. These values were expressed as follows: (major axis/2) x (minor axis/2). For each value, the equivalent diameter (ED) of a circle with the same circumference was calculated in order to have only one reference parameter.

Table I lists mean temperature values measured via the FBG after 50 s from turning the laser on and the diameters of the ducts.

Table I.

Neither extraductal ablation nor surrounding tissue damage were induced.

With both H&E and NADH staining, thermal damage can be appreciated for all *in vivo* tests performed at 7 W, and both for the 3 and 6 min tests (Figure 5). The H&E stain allowed to evaluate if the integrity of common bile duct and cystic duct walls was preserved after LA procedures (Figures 5A, 5C, 5E, 5G). The NADH stain allowed to specifically assess the extension of ablated areas (Figures 5B, 5D, 5F, 5H). In particular, in the case when the cystic duct was treated at 7 W for 6 min, the most superficial layer (mucosal layer) turned out to be completely ablated with no vital tissue left at the NADH stain analysis (Figure 5H). Conversely, with a shorter time application (i.e. 3 min), vital superficial tissue was observed both for the common bile duct and the cystic duct (blue areas in Figures 5B and 5F).

Figure 5.

The *in situ* confocal endomicroscopy evaluation before LA allowed to first evaluate the normal structure of common bile duct and cystic ducts (Figures 6A and 6C). Immediate post-LA evaluation aimed to test the feasibility of confocal endomicroscopy in the recognition of ablation areas (Figures 6E and 6G).
Two main patterns could be identified. Before ablation procedures, the normal tissue appeared as a complex structure with dark cells around glands or vessels (Figures 6A and 6C). Additionally, in the video recorded, erythrocytes could easily be identified circulating through vessels. Conversely, after ablation, the pattern was characterized by a light-grey background consisting in histological architecture distortion and in the disappearance of the gland's contours (Figures

6E and 6G). In addition, no significant erythrocyte activity was detected in the videos. Two independent pathologists were asked to describe the features and to individuate the cells in the Cellvizio® system images, which were extracted from the two videos recorded before thermal treatment. The pixel values of the binary images range from 0 to 255. In the images, the cell nuclei corresponded to black and dark grey pixel values, and are plotted in red in the post-processed images (Figures 6B, 6D, 6F, and 6H). For the common bile duct image, the cell nuclei corresponded to pixel values lower than 90 (Figure 6B). For the cystic duct image, the cell nuclei were indicated as black and dark grey pixels with values lower than 85 (Figure 6D). The same values were used to compute the presence of nuclei in the post-ablation pictures (Figures 6F and 6H), evidencing the complete loss of structure after thermal damage.

Figure 6.

Discussion

The present study represents a step forward in the evaluation of LA thermal effects in the *in vivo* intraductal biliary application. Only one study regarding the ablation of biliary ducts was reported in the literature [31], describing the *ex vivo* application of the Nd:YAG laser light into the cystic ducts of animal models.

The first aim of this study was to evaluate the feasibility of the procedure regarding the absence of anatomical biliary perforation. This was first confirmed by inspecting the surgical field after each LA and later on by performing a histological analysis. For this purpose, the H&E stain was used. As shown in Figure 4, no perforation was detected in any case, irrespective of the laser settings used. Although modifications caused by thermal damage were evident, the full-thickness of the wall was preserved in all cases.

As second and third outcomes, local thermal monitoring and thermal damage assessment, according to different laser settings, were mandatory. These data supported whether the desired thermal damage could be achieved in a safe setting. In particular, the measurement of tissue temperature increase was useful to verify that a cytotoxic temperature was reached and maintained during the whole LAs. The choice of using a FBG sensor is mainly related to the

promising results already obtained in the LA field [24, 39, 40]. For instance, their small size, flexibility and lightness, in addition to good metrological characteristics [41, 42], and the absence of direct light absorption [24] further the combined use with a fiber-optic applicator. The average value of temperature monitored at the interface between the emitting surface of the fiber and the internal duct walls was always above 53°C, and maintained almost constantly after 50 s from turning the laser on. The only exception was noted for the cystic duct test, which lasted 6 min (Figure 3D), in which a sudden and steep temperature increase occurred 1 minute before turning the laser off. The results th

.at we obtained confirmed the achievement of the cytotoxic temperature value with subsequent thermal damage. In addition, a further thermal damage evaluation was also performed by means of *in situ* endomicroscopy and with the histopathological analysis using the NADH stain. A substantial difference before and after LA can be appreciated at endomicroscopy evaluation. As compared to the pre-LA endomicroscopic appearance in which cells were clearly appreciated, the post-LA evaluation revealed a cell structure distortion represented by 'ghost cells', which was then described through a change of pixel values. However, the low depth of penetration of the Cellvizio® system (60µm), led to only differentiate ablated and non-ablated areas, whereas a real depth analysis of damage could not be obtained. As a result, the endomicroscopy system analysis could be mainly useful in the post-ablative evaluation of residual superficial cells as compared to the evaluation of longitudinal ablation spread. So far, the usefulness of the endomicroscopic analysis has already been reported in relation to the real-time detection of cholangiocarcinoma [44, 45]. However, no data were reported regarding its specificity and sensibility in detecting post-procedural cholangiocarcinoma residual cells. Further studies could be required to assess its potentiality as a post-LA evaluation device [46, 47].

Significant and conclusive results were also obtained with a histopathological evaluation using the NADH stain. The loss of succinic acid dehydrogenase activity as an indirect sign of coagulative necrosis allowed to accurately define the spreading width of thermal damage obtained. Particularly, mucosal layer

ablation was clearly achieved in all cases, with a different grade of involvement according to the laser setting used and to the diameter of the ducts. As shown in Figure 5, a major ablation spread was reached for a longer time of application (6 min), with a complete circumferential mucosal involvement in case of smaller diameter ducts (e.g. cystic duct, ED=1.04mm). The optical applicator (diameter of the glass capillary: 1.2 mm) fitted this cystic duct perfectly, and this was particularly true because of the elastic properties of duct walls. This could have helped to achieve a complete circumferential ablation. Conversely, residual vital tissue was observed in case of a shorter time of application (3 min) both for the common bile duct and the cystic duct. This drawback is due to the diameters of the ducts, which are 3.24mm and 1.95mm for the two common bile ducts under test, and 1.16mm for one cystic duct.

Since each subject has a different duct diameter [33], the abovementioned issue could be easily overcome by using a laser probe which adapts to the internal diameter of the ducts. For instance, the probe can be equipped with a balloon in correspondence to the irradiation part. It can be insufflated with a saline solution, which guarantees an homogeneous contact with the duct internal wall [31].

The evaluation of the nature of the damage deserves attention. In the proposed study, it was not possible to accurately distinguish between reversible and non-reversible thermal damage. The animals were euthanized immediately after the ablations, and the duct samples were resected within the following 30 minutes from the treatment to perform the histology evaluation [48]. Since the aim of LA is to produce non-reversible thermal injury in the target, further studies will be designed to evaluate the effectiveness of LA.

Conclusions

In our *in vivo* experiments, we demonstrated the feasibility of biliary tree LA. The integration of FBG technology with a diode laser applicator allowed for a real-time temperature monitoring during thermal treatment. This ability to yield continuous local temperature information would successfully testify to multiple

clinical benefits. The accurate temperature detected would be the representation of the extension of the ablated areas reached, and would indirectly yield information on the necessity to have multiple applications for complete tumor cell destruction. To do so, an adjunctive effort could be made with the contextual use of the endomicroscopy imaging system. However, further tests should be performed to better define appropriate laser settings to use in relation to duct diameter where an ablation is performed, in order to guarantee the optimal thermal damage of the targeted area.

Disclosures

The authors have no relevant financial interests in this article and no potential conflicts of interest to disclose.

Acknowledgments

The authors would like to thank Guy Temporal and Christopher Burel for their assistance in proofreading the manuscript.

This research was partially supported by the IHU-Strasbourg, under the I-Thermo LAP grant.

Text word count: 4121

References

1. DeOliveira ML, Cunningham SC, Cameron JL, et al. Cholangiocarcinoma: thirty-one-year experience with 564 patients at a single institution. Ann Surg. 2007 May;245(5):755-62. doi: 10.1097/01.sla.0000251366.62632.d3. PubMed PMID: 17457168; PubMed Central PMCID: PMCPMC1877058.
2. Valle JW. Advances in the treatment of metastatic or unresectable biliary tract cancer. Ann Oncol. 2010 Oct;21 Suppl 7:vii345-8. doi: 10.1093/annonc/mdq420. PubMed PMID: 20943640.
3. Cunningham SC, Choti MA, Bellavance EC, et al. Palliation of hepatic tumors. Surg Oncol. 2007 Dec;16(4):277-91. doi: 10.1016/j.suronc.2007.08.010. PubMed PMID: 17935975.
4. Kahaleh M. Photodynamic therapy in cholangiocarcinoma. J Natl Compr Canc Netw. 2012 Oct 01;10 Suppl 2:S44-7. PubMed PMID: 23055215.
5. Boulay BR, Gardner TB, Gordon SR. Occlusion rate and complications of plastic biliary stent placement in patients undergoing neoadjuvant chemoradiotherapy for pancreatic cancer with malignant biliary obstruction. J

Clin Gastroenterol. 2010 Jul;44(6):452-5. doi: 10.1097/MCG.0b013e3181d2ef06. PubMed PMID: 20179612.
6. Bertani H, Frazzoni M, Mangiafico S, et al. Cholangiocarcinoma and malignant bile duct obstruction: A review of last decades advances in therapeutic endoscopy. World J Gastrointest Endosc. 2015 Jun 10;7(6):582-92. doi: 10.4253/wjge.v7.i6.582. PubMed PMID: 26078827; PubMed Central PMCID: PMCPMC4461933.
7. Rustagi T, Jamidar PA. Intraductal radiofrequency ablation for management of malignant biliary obstruction. Dig Dis Sci. 2014 Nov;59(11):2635-41. doi: 10.1007/s10620-014-3237-9. PubMed PMID: 24906696.
8. Sharaiha RZ, Natov N, Glockenberg KS, et al. Comparison of metal stenting with radiofrequency ablation versus stenting alone for treating malignant biliary strictures: is there an added benefit? Dig Dis Sci. 2014 Dec;59(12):3099-102. doi: 10.1007/s10620-014-3264-6. PubMed PMID: 25033929.
9. Zoepf T. Photodynamic therapy of cholangiocarcinoma. HPB (Oxford). 2008;10(3):161-3. doi: 10.1080/13651820801992625. PubMed PMID: 18773045; PubMed Central PMCID: PMCPMC2504366.
10. Zoepf T, Jakobs R, Arnold JC, et al. Palliation of nonresectable bile duct cancer: improved survival after photodynamic therapy. Am J Gastroenterol. 2005 Nov;100(11):2426-30. doi: 10.1111/j.1572-0241.2005.00318.x. PubMed PMID: 16279895.
11. Cheon YK. The role of photodynamic therapy for hilar cholangiocarcinoma. Korean J Intern Med. 2010 Dec;25(4):345-52. doi: 10.3904/kjim.2010.25.4.345. PubMed PMID: 21179270; PubMed Central PMCID: PMCPMC2997961.
12. Smith I, Kahaleh M. Biliary Tumor Ablation with Photodynamic Therapy and Radiofrequency Ablation. Gastrointest Endosc Clin N Am. 2015 Oct;25(4):793-804. doi: 10.1016/j.giec.2015.06.013. PubMed PMID: 26431605.
13. Pereira S, Hughes S, Roughton M, et al. Photostent-02; porfimer sodium photodynamic therapy plus stenting versus stenting alone in patients (pts) with advanced or metastatic cholangiocarcinomas and other biliary tract tumours (BTC): a multicentre, randomised phase III trial. ANNALS OF ONCOLOGY. 2010;21:250-250.
14. Dowlatshahi K, Bhattacharya AK, Silver B, et al. Percutaneous interstitial laser therapy of a patient with recurrent hepatoma in a transplanted liver. Surgery. 1992 Sep;112(3):603-6. PubMed PMID: 1325675.
15. Huang GT, Wang TH, Sheu JC, et al. Low-power laserthermia for the treatment of small hepatocellular carcinoma. Eur J Cancer. 1991;27(12):1622-7. PubMed PMID: 1664220.
16. Nolsoe CP, Torp-Pedersen S, Burcharth F, et al. Interstitial hyperthermia of colorectal liver metastases with a US-guided Nd-YAG laser with a diffuser tip: a pilot clinical study. Radiology. 1993 May;187(2):333-7. doi: 10.1148/radiology.187.2.8475269. PubMed PMID: 8475269.
17. Pacella CM, Bizzarri G, Francica G, et al. Analysis of factors predicting survival in patients with hepatocellular carcinoma treated with percutaneous laser ablation. J Hepatol. 2006 May;44(5):902-9. doi: 10.1016/j.jhep.2006.01.031. PubMed PMID: 16545480.
18. Vogl TJ, Muller PK, Hammerstingl R, et al. Malignant liver tumors treated with MR imaging-guided laser-induced thermotherapy: technique and

prospective results. Radiology. 1995 Jul;196(1):257-65. doi: 10.1148/radiology.196.1.7540310. PubMed PMID: 7540310.
19. Pacella CM, Bizzarri G, Spiezia S, et al. Thyroid tissue: US-guided percutaneous laser thermal ablation. Radiology. 2004 Jul;232(1):272-80. doi: 10.1148/radiol.2321021368. PubMed PMID: 15155898.
20. Di Matteo F, Picconi F, Martino M, et al. Endoscopic ultrasound-guided Nd:YAG laser ablation of recurrent pancreatic neuroendocrine tumor: a promising revolution? Endoscopy. 2014;46 Suppl 1 UCTN:E380-1. doi: 10.1055/s-0034-1377376. PubMed PMID: 25254586.
21. Matthewson K, Coleridge-Smith P, O'Sullivan JP, et al. Biological effects of intrahepatic neodymium:yttrium-aluminum-garnet laser photocoagulation in rats. Gastroenterology. 1987 Sep;93(3):550-7. PubMed PMID: 3609664.
22. Ishikawa T, Zeniya M, Fujise K, et al. Clinical application of Nd:YAG laser for the treatment of small hepatocellular carcinoma with new shaped laser probe. Lasers Surg Med. 2004;35(2):135-9. doi: 10.1002/lsm.20071. PubMed PMID: 15334617.
23. Vogl TJ, Straub R, Eichler K, et al. Colorectal carcinoma metastases in liver: laser-induced interstitial thermotherapy--local tumor control rate and survival data. Radiology. 2004 Feb;230(2):450-8. doi: 10.1148/radiol.2302020646. PubMed PMID: 14688400.
24. Saccomandi P, Schena E, Silvestri S. Techniques for temperature monitoring during laser-induced thermotherapy: an overview. Int J Hyperthermia. 2013 Nov;29(7):609-19. doi: 10.3109/02656736.2013.832411. PubMed PMID: 24032415.
25. Schena E, Tosi D, Saccomandi P, et al. Fiber Optic Sensors for Temperature Monitoring during Thermal Treatments: An Overview. Sensors (Basel). 2016 Jul 22;16(7). doi: 10.3390/s16071144. PubMed PMID: 27455273; PubMed Central PMCID: PMCPMC4970186.
26. Manns F, Milne PJ, Gonzalez-Cirre X, et al. In situ temperature measurements with thermocouple probes during laser interstitial thermotherapy (LITT): quantification and correction of a measurement artifact. Lasers Surg Med. 1998;23(2):94-103. PubMed PMID: 9738544.
27. Gassino R, Liu Y, Konstantaki M, et al. A fiber optic probe for tumor laser ablation with integrated temperature measurement capability. Journal of Lightwave Technology. 2017;35(16):3447-3454.
28. Polito D, Caponero MA, Polimadei A, et al. A needlelike probe for temperature monitoring during laser ablation based on fiber Bragg grating: Manufacturing and characterization. Journal of Medical Devices. 2015;9(4):041006.
29. Di Santo N, Cavaiola C, Saccomandi P, et al., editors. Feasibility assessment of an FBG-based probe for distributed temperature measurements during laser ablation. Medical Measurements and Applications (MeMeA), 2016 IEEE International Symposium on; 2016: IEEE.
30. Schena E, Saccomandi P, Fong Y. Laser Ablation for Cancer: Past, Present and Future. J Funct Biomater. 2017 Jun 14;8(2). doi: 10.3390/jfb8020019. PubMed PMID: 28613248; PubMed Central PMCID: PMCPMC5492000.
31. Rea R, Di Matteo FM, Martino M, et al. Endoluminal Nd:YAG laser application in ex vivo biliary porcine tissue. Lasers Med Sci. 2017 Aug;32(6):1411-1415. doi: 10.1007/s10103-017-2264-0. PubMed PMID: 28667507.

32. Rao Y-J. Fiber Bragg grating sensors: principles and applications. Optical fiber sensor technology: Springer; 1998. p. 355-379.
33. Schwartz S, Brunicardi, FC. Schwartz's principles of surgery. 9th ed. McGraw-Hill, editor. New York (NY)2010.
34. Yarmolenko PS, Moon EJ, Landon C, et al. Thresholds for thermal damage to normal tissues: an update. Int J Hyperthermia. 2011;27(4):320-43. doi: 10.3109/02656736.2010.534527. PubMed PMID: 21591897; PubMed Central PMCID: PMCPMC3609720.
35. Dewhirst MW, Viglianti BL, Lora-Michiels M, et al. Basic principles of thermal dosimetry and thermal thresholds for tissue damage from hyperthermia. Int J Hyperthermia. 2003 May-Jun;19(3):267-94. doi: 10.1080/0265673031000119006. PubMed PMID: 12745972.
36. http://pdf.medicalexpo.com/pdf/mauna-kea-technologies/cellvizio/81216-151882.html - open.
37. Kiesslich R, Duckworth C, Moussata D, et al. Local barrier dysfunction identified by confocal laser endomicroscopy predicts relapse in inflammatory bowel disease. Gut. 2011:gutjnl-2011-300695.
38. Lim LG, Neumann J, Hansen T, et al. Confocal endomicroscopy identifies loss of local barrier function in the duodenum of patients with Crohn's disease and ulcerative colitis. Inflammatory bowel diseases. 2014;20(5):892-900.
39. Tosi D, Macchi EG, Gallati M, et al. Fiber-optic chirped FBG for distributed thermal monitoring of ex-vivo radiofrequency ablation of liver. Biomed Opt Express. 2014 Jun 01;5(6):1799-811. doi: 10.1364/BOE.5.001799. PubMed PMID: 24940541; PubMed Central PMCID: PMCPMC4052912.
40. Palumbo G, Iadicicco A, Tosi D, et al. Temperature profile of ex-vivo organs during radio frequency thermal ablation by fiber Bragg gratings. J Biomed Opt. 2016 Nov 01;21(11):117003. doi: 10.1117/1.JBO.21.11.117003. PubMed PMID: 27846343.
41. Rao Y, Hurle B, Webb D, et al., editors. In-situ temperature monitoring in NMR machines with a prototype in-fibre Bragg grating sensor system. Optical Fiber Sensors; 1997: Optical Society of America.
42. Samset E, Mala T, Ellingsen R, et al. Temperature measurement in soft tissue using a distributed fibre Bragg-grating sensor system. Minimally Invasive Therapy & Allied Technologies. 2001;10(2):89-93.
43. van Rhoon GC, Samaras T, Yarmolenko PS, et al. CEM43 degrees C thermal dose thresholds: a potential guide for magnetic resonance radiofrequency exposure levels? Eur Radiol. 2013 Aug;23(8):2215-27. doi: 10.1007/s00330-013-2825-y. PubMed PMID: 23553588; PubMed Central PMCID: PMCPMC3799975.
44. Chennat J, Konda VJ, Madrigal-Hoyos E, et al. Biliary confocal laser endomicroscopy real-time detection of cholangiocarcinoma. Dig Dis Sci. 2011 Dec;56(12):3701-6. doi: 10.1007/s10620-011-1795-7. PubMed PMID: 21695400.
45. Slivka A, Gan I, Jamidar P, et al. Validation of the diagnostic accuracy of probe-based confocal laser endomicroscopy for the characterization of indeterminate biliary strictures: results of a prospective multicenter international study. Gastrointest Endosc. 2015 Feb;81(2):282-90. doi: 10.1016/j.gie.2014.10.009. PubMed PMID: 25616752.

46. Schneider C, Johnson SP, Walker-Samuel S, et al. Utilizing confocal laser endomicroscopy for evaluating the adequacy of laparoscopic liver ablation. Lasers in surgery and medicine. 2016;48(3):299-310.
47. Diana M, Schiraldi L, Liu Y-Y, et al. High intensity focused ultrasound (HIFU) applied to hepato-bilio-pancreatic and the digestive system—current state of the art and future perspectives. Hepatobiliary surgery and nutrition. 2016;5(4):329.
48. Thomsen S, Pearce JA. Thermal damage and rate processes in biologic tissues. Optical-thermal response of laser-irradiated tissue: Springer; 2010. p. 487-549.

Table I. Mean temperature values after 50 s from turning the laser on (expressed as mean value ± standard deviation), and diameters of the ducts, expressed as follows: (major axis/2) x (minor axis/2) and equivalent diameter (ED).

	Common bile duct		**Cystic duct**	
Settings	**T mean [°C]**	**Axes [mm^2] (ED [mm])**	**T mean [°C]**	**Axes [mm^2] (ED [mm])**
7 W x 3 min	53±1	3.07x3.42 (3.24)	56±1	1.59x0.84 (1.16)
7 W x 6 min	55±1	4.51x0.84 (1.95)	55±3	1.09x1.00 (1.04)

FIGURE 1

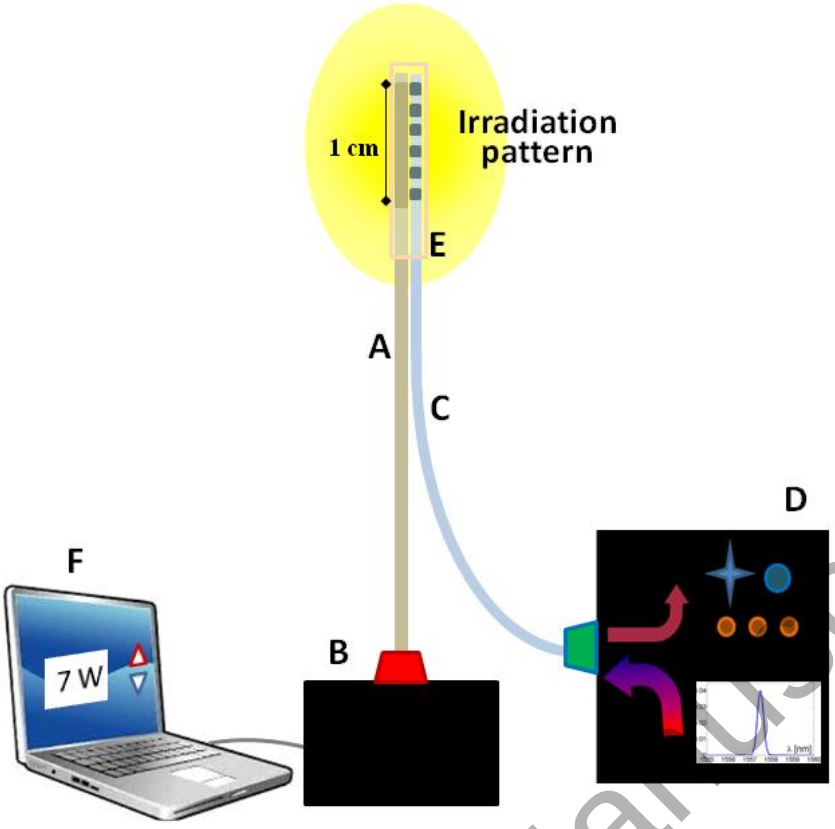

FIGURE 2

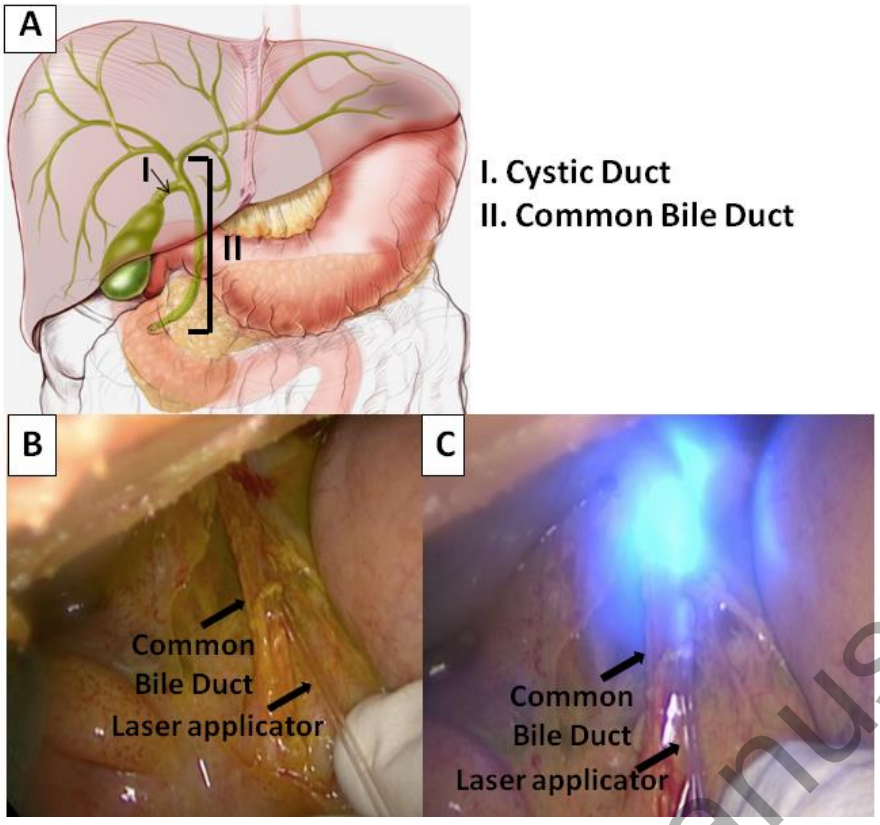

FIGURE 3

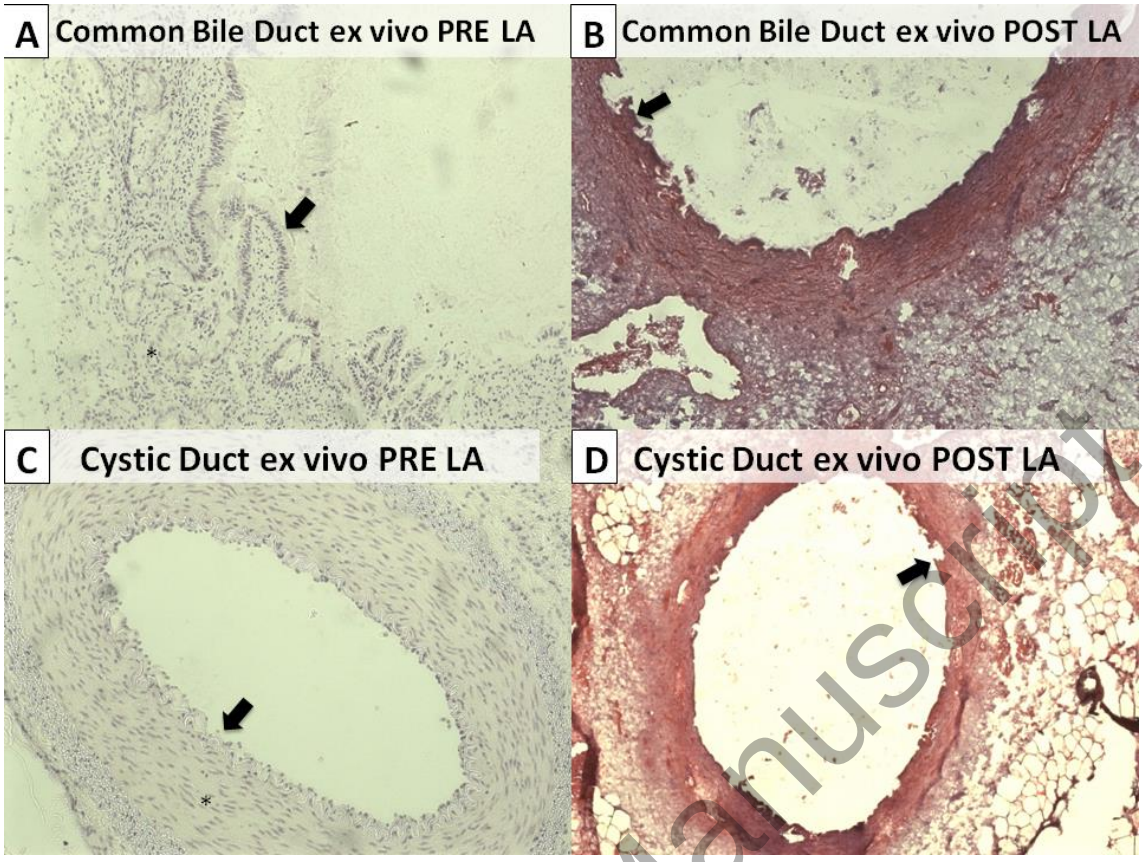

FIGURE 4

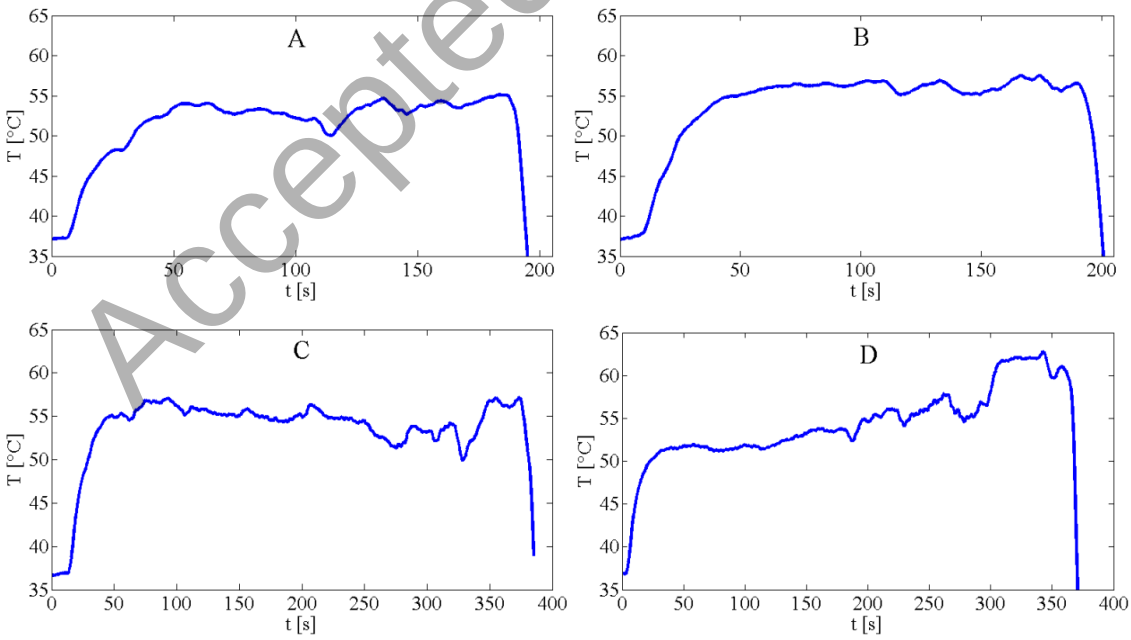

FIGURE 5

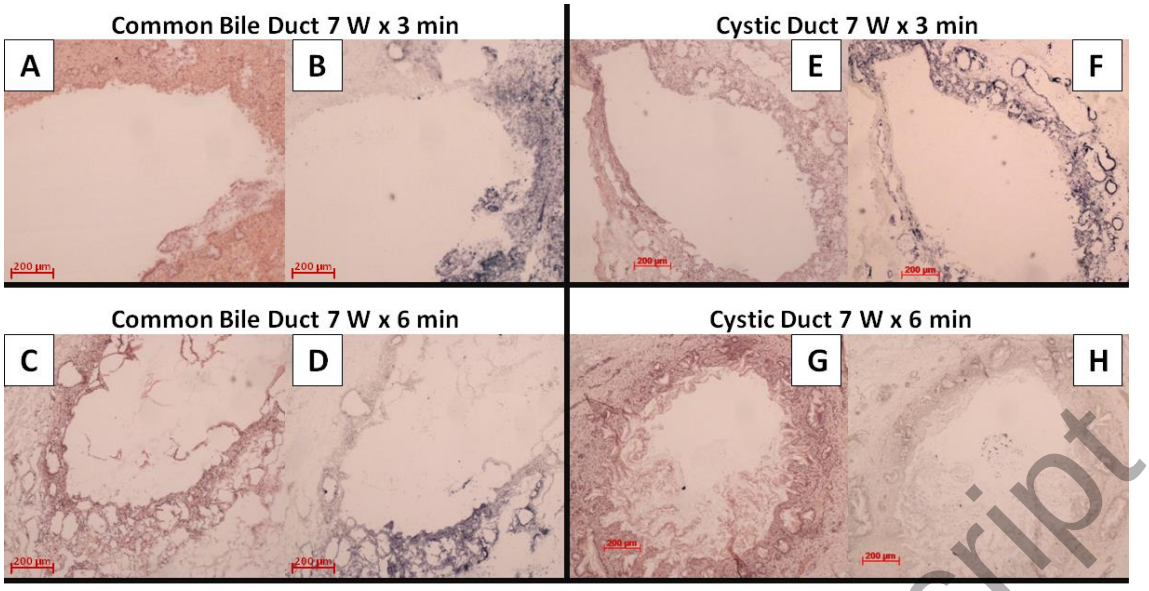

FIGURE 6

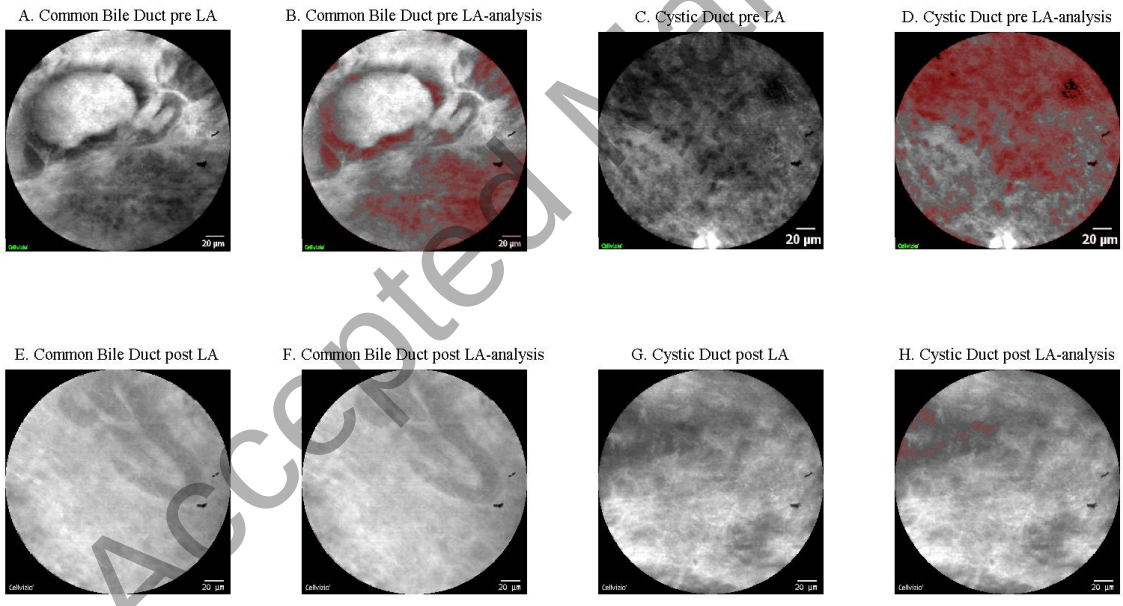

CAPTIONS OF FIGURES:

Figure 1. Schematic of laser delivery and of temperature measuring systems. These include the delivery fiber which guides the high-power laser beam (A) emitted by means of a diode-based laser source (B) to the 1cm emitting area (drawing not in scale), the temperature fiber Bragg grating sensor (C), and the optical interrogator (D). The tips of the delivery fiber and of the FBG are bound together by a glass capillary (E). A laptop (F) is used to control the laser system.

Figure 2. Schematic of biliary tree anatomy (A). Laser applicator insertion into the common bile duct through a 1cm longitudinal incision (B) and LA (C). Pictures were taken using the snapshot function of the laparoscopic camera.

Figure 3. Normal histological structure of the common bile duct. The most superficial layer is organized as a single columnar epithelium, composing pleats and folds (black arrow). The underlying portion is made up of a dense connective tissue (*) (A). Normal histological structures of the cystic duct. The surface epithelium is composed of tall, uniform, and columnar cells (black arrow). Deeper circular, longitudinal, and oblique smooth muscle fibers without distinct layers can be identified (*) (C). Coagulative necrosis of the most superficial portion can be observed for both the common bile duct and cystic duct with rare craters induced by the ablation. Wall integrity turned out to be preserved in both cases (B) and (D).

Figure 4. Temperature trend during LA in the common bile duct (A) and the cystic duct (B) at 7 W for 3 min, and in the common bile duct (C) and the cystic duct (D) at 7 W for 6 min.

Figure 5. Histological samples of common bile duct after H&E (A) and NADH (B) staining at 3 min, and H&E (C) and NADH (D) staining at 6 min. Histological samples of the cystic duct after H&E (E) and NADH (F) staining at 3 min, and H&E (G) and NADH (H) staining at 6 min (Zeiss Axiophot, 5x enlargement).

Figure 6. Confocal images acquired before (A) and after (E) LA in the common bile duct, and before (C) and after (G) ablation in the cystic duct. Image analysis evidenced the red mask plotted in correspondence to the cells visible in the

images before (B) and after (F) LA in the common bile duct and before (D) and after (H) LA in the cystic ducts.